A real-time solution for an inverse Cauchy problem in cardiology*

Ricardo Celorrio† Andreas Hofinger‡

Abstract

The *inverse problem of electrocardiography* describes the reconstruction of the cardiac electrophysiological activity from remote measurements of its generated electrical potential. In this work we present a method to solve this ill-posed problem in real time under simultaneous regularization in time and space. Furthermore we propose a fast post-processing step that recovers the speed of the traveling potential.

Numerical examples are presented to illustrate the robustness and efficiency of the new method.

1 Introduction

In the inverse problem of electrocardiology the aim is to recover electrophysiological activity of the heart without measuring directly on its surface (see [19] for a review). In the classical setup the data are acquired by placing electrodes (typically 64) on the torso surface to recover the epicardial potential [9, 22, 24]. This is a non-invasive technique, but only yields a very low resolution (in particular due to the partly large distance between electrodes and heart). Recently an alternative method has been proposed: Via a catheter a balloon with 64 electrodes on its surface is moved into the right atrium to recover the endocardial potential [29]. The goal is to obtain better reconstructions than with the standard technique.

*This work has been supported by the Austrian National Science Foundation FWF under project grant SFB F 13/08, and by the Spanish projects MEC / FEDER Ref. MTM 2004-019051 and MCYT / FEDER Ref. BFM 2001-2521.

†Universidad de Zaragoza, Zaragoza, Spain, e-mail: celorrio@unizar.es.

‡Johann Radon Institute for Computational and Applied Mathematics (RICAM), Linz, Austria, e-mail: andreas.hofinger@oeaw.ac.at.

Considering the usual model for solving the inverse problem of electrocardiology [11, 19], from the mathematical point of view, both techniques lead to a severely ill-posed problem related to the Laplace equation, where the Cauchy data (potential and electrical field) of the solution are known in a part of the boundary of the physical domain and no information about boundary conditions in the remaining part of the boundary is available. In both cases the measurements cannot be taken directly on the heart surface, and therefore the solution is very sensitive to small errors in data; to solve the problem in a stable way we have to apply regularization techniques.

Concerning the unknown in the inverse problem of electrocardiography there are two different approaches:

Identification of the endocardial potential. This approach is valid for the diagnosis of any dysfunction in the myocardial activity and yields a linear ill-posed problem. In [4] a natural regularization is proposed, where constraints in space and time are imposed; but unfortunately the resulting system is extremely large and therefore very expensive to solve. We present a careful implementation of a similar approach with multiple restrictions in order to obtain the solutions in *real time.*

In [24] a regularization based on inequalities to ensure the monotonic behaviour of the *transmembrane potential pattern (TMP)* is applied. This approach yields a quadratic optimization problem with linear restrictions; as reported in [24] solving this problem takes several hours.

Finally, in [17, 18] it is proposed to interpret the data values as a matrix and apply a singular value decomposition of this matrix (not the operator!) to filter the noise. Nevertheless it is not clear that the noise has any relation with such a decomposition, moreover this approach involves infinitely many regularization parameters without giving a sound rule for determining these.

Identification of the myocardial activation time. In this approach it is assumed that the shape of the TMP is known, and that all cells have the same TMP (also called *activation function*). The latter assumption is valid in healthy tissue and also in some pathological situations, e. g., the Wolf-Parkinson-White syndrome, but is not valid for the important cases of infarcts or ischemia.

In [16, 22] it is shown that knowledge of critical points and critical values of the activation time can in principle be used to stabilize the problem. Nonetheless, the resulting methods are difficult to be implemented in an automated way.

In general, approaches for recovering the activation time directly lead to a reduction of the dimension by one but also to large nonlinear and non-convex optimization problems.

Both approaches were compared in different situations in [8, 9] where it turned out that (under optimal choice of parameters) they perform similarly.

In this work we propose a different strategy: We present an efficient algorithm to solve the problem of the first approach in real-time. Instead of determining the activation time afterwards, we propose to use a post processing step to recover the *velocity of the wave* on the surface. In contrast to the methods described above, it is possible to perform this step without knowledge of the TMP. Moreover, it can again be implemented in real-time, and gives similar information as the activation time in a stable way.

We exemplify the new techniques by applying them to a 2D-problem closely related to the method involving interior measurements on a balloon. This simplified problem still contains the essential complications of the corresponding 3D problems, especially those associated to the number of unknowns and the computation time; furthermore the singular values decay equally fast. The main difference is that determining a tangential derivative in the 2D problem is more straightforward than the computation of surface derivatives in a 3D problem.

Another point we want to discuss is the choice of regularization parameters. A crucial point is to choose these parameters such that the aspiration "the lower the noise level, the more accurate the solution" is fulfilled, i. e., for the solution of this problem a convergent regularization strategy [13] should be used. In the context of the inverse problem of endocardiology very often noise free strategies are applied to choose regularization parameters (e. g. [4, 8, 9, 11, 17, 18, 24]). In section 3 we want to recall that noise free methods can never yield convergent regularization methods in the sense mentioned above, the deeper reason behind this fact is a classical result due to Bakushinskii [2]. In contrast the discrepancy principle yields convergence rates of optimal order.

This report is organized as follows. In sections 2 and 3 we present theoretical results on the behavior of the forward and the inverse problem, and show that under weak assumptions on the true solution the discrepancy principle yields an order-optimal rate of convergence. The main results of this paper are contained in sections 4 and 5 where we describe how the linear problem can be solved in real-time, and how the speed of the wave can be detected without knowledge of the shape of the TMP. Finally numerical examples are given in section 6 to illustrate the efficiency and robustness of the new method. The appendix contains the proof of one of the theorems and a detailed description of the boundary element method that is used in order to solve the inverse problem.

In the next section we analyze properties of the forward operator, i. e., the operator that maps a potential on the endocardium to a corresponding measurement on the balloon.

2 Forward Problem

The forward problem we now consider is the mapping of potentials on the surface of the heart onto corresponding potentials on the balloon. Although the electrocardial potential changes over time, we can deal with a sequence of electrostatic problems, instead of an electrodynamic one—the time dependence is due to chemical reactions and cell-to-cell interaction, not due to electrodynamic effects.

The proper model of the problem under consideration is Laplace's equation in $\Omega \subset \mathbb{R}^3$, where Ω is a smooth deformation of the set $\{x \in \mathbb{R}^3 \mid 1/2 < \|x\| < 1\}$, and $\partial\Omega = \Gamma_o \cup \Gamma_i$, with Dirichlet conditions on the outer boundary Γ_o and Neumann conditions on the inner boundary Γ_i.

The forward problem can be formulated via the following boundary value problem

$$\Delta u = 0 \quad \text{in } \Omega \tag{1a}$$

$$u = u_o \quad \text{on } \Gamma_o \tag{1b}$$

$$\frac{\partial u}{\partial \nu} = 0 \quad \text{on } \Gamma_i \tag{1c}$$

where $\partial/\partial\nu$ denotes the normal derivative. The unknown is $u_i := u|_{\Gamma_i}$, the potential on the balloon.

The Neumann-condition (1c) on the balloon is due to current conservation: since the balloon is insulated, no current can flow through its boundary and any current close to it must be tangential to the surface. Since blood is a conducting fluid, we obtain via Ohm's law that also the electrical field near the balloon is tangential (cf. [10]).

In order to show the main difficulties and some powerful techniques to solve the inverse problem explained in section 3, we investigate a closely related

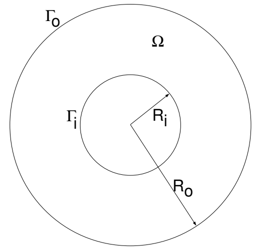

Figure 1: Domain of the test problem.

two-dimensional problem. We want to emphasize that all methods proposed in the following can be implemented such that—given the same number of electrodes—there is no significant increase in the computation time when they are applied to the full 3D-setting.

So from now on we consider a 2D test problem as shown in Figure 1. The inner and the outer boundary Γ_i and Γ_o now correspond to concentric circles with radii R_i and R_o respectively.

The forward problem is to determine the potential u on Γ_i (the balloon), given u_o on Γ_o (the endocardium). This problem can be formulated via a linear operator A, which maps a function u_o on Γ_o to the corresponding potential u_i on Γ_i.

$$\begin{aligned} A : L_2(\Gamma_o) &\to L_2(\Gamma_i) \\ u_o &\mapsto u_i := u|_{\Gamma_i} \quad \text{where } u \text{ solves problem (1)} \end{aligned} \tag{2}$$

Due to the radial setup of problem (1), it can be solved analytically by separation of variables, to this end we need Fourier-series.

Notation 2.1 (Fourier-series). For the coefficients of the Fourier-series of a 2π-periodic function u in $L_2([0, 2\pi])$ we use the following convention

$$\begin{aligned} \widehat{u}^{(0)} &= \frac{1}{\pi}\int_0^{2\pi} u(x)\,dx \\ \widehat{u}^{(\mathrm{o},i)} &= \frac{1}{\pi}\int_0^{2\pi} u(x)\sin(ix)\,dx \\ \widehat{u}^{(\mathrm{e},i)} &= \frac{1}{\pi}\int_0^{2\pi} u(x)\cos(ix)\,dx \end{aligned} \tag{3}$$

where the superscripts “o” and “e” denote odd and even coefficients. The Fourier-series of u is than given as

$$u(x) = \frac{\widehat{u}^{(0)}}{2} + \sum_{i=1}^{\infty} \widehat{u}^{(\mathrm{o},i)} \sin(ix) + \sum_{i=1}^{\infty} \widehat{u}^{(\mathrm{e},i)} \cos(ix)$$

where the equality holds in the L_2-sense.

With this setting we are able to give explicit expressions for the solution of the forward problem.

Theorem 2.2. *Let u_o be given on Γ_o and u denote the solution of problem* (1) *with Ω as in Figure 1. Then u_i can be computed via its Fourier series, the coefficients are given as*

$$\widehat{u_i}^{(\cdot,n)} = \rho^n \frac{2}{1+\rho^{2n}} \widehat{u_o}^{(\cdot,n)} \qquad \text{for} \quad n \geq 0 \tag{4a}$$

$$\frac{\widehat{\partial u_o}}{\partial \nu}^{(\cdot,n)} = \frac{n}{R_o} \frac{\rho^n - \rho^{-n}}{\rho^n + \rho^{-n}} \widehat{u_o}^{(\cdot,n)} \quad \text{for} \quad n \geq 0 \tag{4b}$$

where $\widehat{u_i}^{(\cdot,n)}$ denotes the n-th Fourier coefficient of the 2π-periodic function $u_i(t) := u(R_i \cos(t), R_i \sin(t))$ and $\rho := R_i/R_o$ is the ratio of outer and inner radius.

Proof. Formulating equation (1a) in polar coordinates (with radius r and angle φ) it can be seen easily that the functions

$$1, \quad \log(r), \quad r^n \sin(n\varphi), \quad r^n \cos(n\varphi) \quad \text{for} \quad n = \pm 1, \pm 2, \ldots \tag{5}$$

are solutions of Laplace's equation on the annulus. Applying Gauß' theorem

$$\oint_{\Gamma_i \cup \Gamma_o} u \frac{\partial v}{\partial \nu} - v \frac{\partial u}{\partial \nu} = \int_\Omega u \Delta v - v \Delta u$$

to the solution u of (1) and functions v as in (5) we obtain an identity for the integrals along Γ_i and Γ_o. Inserting the boundary conditions (1b) and (1c) into this identity yields

$$\int_{\Gamma_o} u_o \frac{\partial v}{\partial \nu} - \int_{\Gamma_o} v \frac{\partial u}{\partial \nu} = \int_{\Gamma_i} u \frac{\partial v}{\partial \nu}.$$

Inserting functions v as in (5), this gives a decoupled system of linear equations for the Fourier-coefficients of u and $\partial u/\partial \nu$. Solving this system we obtain (4). □

According to this theorem we can formally define the operator A that maps u_o to u_i as

$$\begin{aligned} A : L_2(\Gamma_o) &\to L_2(\Gamma_i) \\ u_o &\mapsto u_i := \mathcal{F}^{-1} \Sigma \mathcal{F} u_o, \end{aligned} \tag{6}$$

where the operator Σ denotes multiplication of the nth Fourier coefficient with the corresponding factor in (4a).

Remark 2.3 (Structure of singular values). Note the different decay properties of the factors in (4a) and (4b). Taking the normal derivative of u_o in (4b) is approximately equal to multiplication of the nth Fourier-coefficient of u_o with n, hence this is a *mildly* ill-posed problem. In contrast, propagation from the outer to the inner boundary in (4a) corresponds to multiplication with ρ^n, i. e., this process is exponentially smoothing; the corresponding inverse problem of propagating from the inner to the outer boundary is *severely* ill-posed. For the numerical example considered in section 6 we have $\rho = 0.5$, therefore e. g., an error in the 10th Fourier component would be amplified by the factor 512. This (exponential) increase of the coefficients will not change when the test problem is replaced by a less symmetric geometry or the 3D-case (cf. also [15]).

Already this short amount of analysis indicates that it will not be possible to obtain highly accurate reconstructions of the potential when noise is present. In the next section we give a detailed analysis of the inverse problem and show which type of convergence rates are achievable.

3 Inverse Problem

In this section we turn to theoretical investigations of the inverse problem. Here the goal is to recover the potential on the endocardium, given the measured potential on the balloon, and the physical Neumann-boundary condition (1c). The resulting equations describe a *Cauchy problem* for the Laplace equation where the unknown is u on Γ_o (see also [14]).

$$\left.\begin{aligned} \Delta u &= 0 \quad \text{in } \Omega \\ u &= f \quad \text{on } \Gamma_i \\ \frac{\partial u}{\partial \nu} &= 0 \quad \text{on } \Gamma_i \end{aligned}\right\} \tag{IP}$$

The main difference to equation (1) is that both boundary conditions are stated on Γ_i, which has dramatic influence on the behavior of the solutions. Solving problem (IP) for u on Γ_o is equivalent to inversion of the operator A in (6); the singular values of this operator tend to zero as $\mathcal{O}(\rho^n)$, therefore this inversion is exponentially (or severely) ill-posed.

In practice not the exact right hand side f of (IP) will be available, but only a noisy version[1] f^δ, with $\left\|f - f^\delta\right\| \leq \delta$. Hence, in order to solve (IP) we

[1]Not only measurement errors are an issue here, but also uncertainty due to incomplete/inexact knowledge of the geometry of the heart or the position of the balloon (cf. also [9]).

have to apply a regularization technique, in particular we consider Tikhonov-regularization. Here, instead of solving the equation $Au = f^\delta$, we minimize a related functional:

$$\left\|Au - f^\delta\right\|^2 + \alpha \left\|u\right\|^2 \to \min\,, \tag{7}$$

the corresponding solution is denoted by u_α^δ.

A crucial point when (7) is solved, is the correct choice of the regularization parameter α. If α is chosen too small then we will obtain unstable solutions, if α is too large, the results will be very smooth and stable, but bad approximations to the true solution. Morozov's discrepancy principle suggests to choose the regularization parameter such that the residual is of the same order of magnitude as the noise level.

Remark 3.1 (Discrepancy Principle). Choose the largest regularization parameter $\alpha = \alpha(\delta, f^\delta)$, $\alpha \le \exp(-1)$ for which the regularized solution u_α^δ satisfies

$$\left\|Au_\alpha^\delta - f^\delta\right\| \le \tau\delta \tag{8}$$

with some $\tau > 1$.

Hohage [21] has shown that for severely ill-posed problems the discrepancy principle yields order optimal convergence rates. Although being optimal, due to the fast decay of the singular values of A together with the weak smoothness condition fulfilled by $u^\dagger$, the resulting convergence rates are only logarithmic. The proof of the following theorem is given in appendix A.

Theorem 3.2. *Let $u^\dagger \in H^p(\Gamma_o)$ and α be chosen according to the discrepancy principle* (8)*, then for noise level $\delta \to 0$ we obtain the convergence rate*

$$\left\|u^\dagger - u_\alpha^\delta\right\|_{L_2(\Gamma_o)} = \mathcal{O}\left((-\ln(\delta))^{-p}\right)\,.$$

Since a typical value for p is e. g., $p = 3/2 - \varepsilon$ (see appendix A), the resulting convergence rate is rather slow. This again indicates that it will not be possible to reconstruct sharp features of the potential.

Theorem 3.2 shows that the discrepancy principle yields an order optimal convergence rate; but in the inverse problem of electrocardiology also other parameter choice rules are widely used. Another common method for choosing the regularization parameter in this context is the L-curve method (used e. g., in [4, 8, 9, 24]). The L-curve method is a so called *error-free method*, i. e., a method that does not utilize information about the noise level. We want to point out that the L-curve method (as well as any other error free method) cannot yield a convergent regularization method, in particular it can never yield results of the form of Theorem 3.2 (this general result is contained in a famous paper by Bakushinskii [2]; for further remarks on the L-curve method see also [12, 20, 28]).

Furthermore we would like to mention that the point of maximum curvature is often determined by hand; in contrast, in [13, Chap. 9] efficient algorithms are proposed to determine the regularization parameters for the discrepancy principle as well as the L-curve method in an automated way.

4 Efficient Regularization in Space and Time

By a priori information related to real data, we may assume that $u(x, \cdot)$ is at least piecewise differentiable, but as we will see in section 6 the numerical solutions obtained by standard Tikhonov regularization (7) are not smooth with respect to time, although they are very smooth in x-direction. A natural next step is therefore to consider penalties on higher order Sobolev norms in time. Fortunately, there is an efficient way to couple all the time-steps, when an L_2-penalty with respect to space, and an H^s-penalty with respect to time is used (cf. also [27]). Utilizing additional knowledge about the singular values of A we can even implement higher order penalties in space efficiently.

In the following we consider an equation of the form

$$Au(\cdot, t) = f(\cdot, t) \quad \text{for all } t, \tag{9}$$

where the linear operator A does not depend on the time variable. We solve problem (9) using simultaneous regularization in space and time, in particular we consider the minimization problem

$$\|\tilde{A}u - f\|^2_{L_2(\Gamma_i \times T)} + \alpha \|u\|^2_{L_2(\Gamma_o \times T)} + \beta \|Du\|^2_{L_2(\Gamma_o \times T)} \to \min_u, \tag{10}$$

where $\tilde{A} : L_2(\Gamma_o \times T) \to L_2(\Gamma_i \times T)$ is the pointwise extension of the operator A and D is a differential operator with respect to time t. Under the assumption that we know a singular system (σ_n, w_n, v_n) of A, i. e.,

$$\begin{aligned} Av_n &= \sigma_n w_n \\ A^* w_n &= \sigma_n v_n \end{aligned} \tag{11}$$

For the small problem sizes under consideration ($n_g = 64$ electrodes) such a singular system can be computed numerically at a negligible cost, the contribution to the total computation time in section 6 is less than 1%.

Theorem 4.1. *Let (σ_n, w_n, v_n) be a singular system of A, then the minimizing element u of* (10) *is given as*

$$u(x,t) = \sum\nolimits_n \Big(\sigma_n \left((\sigma_n^2 + \alpha) I + \beta D^* D \right)^{-1} \left\langle f(\cdot, t),\, w_n(\cdot) \right\rangle \Big) v_n(x). \quad (12)$$

Proof. Observe that for arbitrary t the minimizer $u(\cdot,t)$ of the functional in (10) is necessarily an element of $\mathcal{N}(A)^\perp$ and that it does only depend on the projection of $f(\cdot,t)$ onto $\overline{\mathcal{R}(A)}$. Hence, without loss of generality we may assume $f(\cdot,t) \in \overline{\mathcal{R}(A)}$ and expand u and f in Fourier-series with respect to the orthogonal function system in (11):

$$u(x,t) = \sum_n \langle u(\cdot,t),\, v_n(\cdot)\rangle\, v_n(x) \;\; =: \sum_n u_n(t) v_n(x) \quad (13)$$

$$f(x,t) = \sum_n \langle f(\cdot,t),\, w_n(\cdot)\rangle\, w_n(x) =: \sum_n f_n(t) w_n(x) \quad (14)$$

If we plug these relations into (10) we obtain

$$\int_T \int_{\Gamma_i} \bigg(\Big(A \sum\nolimits_n u_n(t) v_n(x) \Big) - \sum\nolimits_n f_n(t) w_n(x) \bigg)^2 \quad (15)$$

$$+ \int_{\Gamma_o} \alpha \bigg(\sum\nolimits_n u_n(t) v_n(x) \bigg)^2 + \beta \bigg(\sum\nolimits_n \big(D u_n(t)\big) v_n(x) \bigg)^2 \, dx\, dt \to \min$$

Using (11) and the orthogonality relations $\langle v_m,\, v_n\rangle = \delta_{mn}$ and $\langle w_m,\, w_n\rangle = \delta_{mn}$, expression (15) simplifies to

$$\int_T \sum_n \big(\sigma_n u_n(t) - f_n(t)\big)^2 + \alpha \sum_n u_n(t)^2 + \beta \sum_n \big(D u_n(t)\big)^2 dt \to \min \quad (16)$$

This minimum is attained if and only if it is attained individually for each n. The resulting equations can now easily be solved and we obtain (12). $\square$

In [4] it has been proposed to not only use penalties on derivatives in time but also on derivatives in space in (10). Unfortunately, if a penalty on space derivatives is used we cannot perform a diagonalization as in Theorem 4.1.

Nevertheless, due to the results of section 2 and Proposition A.1 in the appendix we are able to add a penalty that has the same properties as differentiation, but does commute with the operator A: Instead of adding a penalty of the form $\gamma \|u\|_{L_2(T, H^p(\Gamma_o))}$ to (10), we consider the functional

$$\|\tilde{A}u - f\|^2 + \alpha \|u\|^2 + \beta \|Du\|^2 + \gamma \|1/\varphi_p(\tilde{A}^* \tilde{A}) u\|^2 \to \min_u, \quad (17)$$

According to Proposition A.1 we know that the operator $1/\varphi_p(A^*A)$ generates the same norm as p times differentiating, and thus the last term just generates the $L_2(T, H^p(\Gamma_o))$-norm. For this modified problem again an efficient formula for computing u is available.

Theorem 4.2. *Let (σ_n, w_n, v_n) be a singular system of A, then the minimizing element u of* (17) *is given as*

$$u(x,t) = \sum_n \Big(\sigma_n \left(\left(\sigma_n^2 + \alpha + \gamma/\varphi_p(\sigma_n^2) \right) I + \beta D^* D \right)^{-1} \left\langle f(\cdot,t),\, w_n(\cdot) \right\rangle \Big) v_n(x). \tag{18}$$

In the following remark we describe how the solution of (10) is computed numerically after discretization.

Remark 4.3 (Implementation of dynamic regularization). If we denote the matrix corresponding to the operator A by $\mathbf{A}$, the algorithm for computing $(\mathbf{u})_{i,j} \approx u(x_i, t_j)$ is given as follows:

- Setup the matrix $\mathbf{A}$ as described in appendix B and compute the singular value decomposition $\mathbf{A} = \mathbf{U}\boldsymbol{\Sigma}\mathbf{V}^T$, $\boldsymbol{\Sigma} = \mathrm{diag}(\sigma_1, \ldots, \sigma_{n_g})$.
- Transform the data $(\mathbf{F})_{i,j} := f^\delta(x_i, t_j)$ via

  $$\hat{\mathbf{F}} = \mathbf{U}^T \mathbf{F}$$

- Compute an intermediate solution $\hat{\mathbf{u}}$ as

  $$\hat{\mathbf{u}} = \sum_{n=1}^{n_g} \sigma_n \left((\sigma_n^2 + \alpha)\mathbf{I} + \mathbf{D}^T\mathbf{D} \right)^{-1} \hat{\mathbf{F}}$$

- Transform the result to obtain the regularized solution $\mathbf{u}$

  $$\mathbf{u} = \mathbf{V}\hat{\mathbf{u}}$$

If the operator $\mathbf{D}$ represents differentiating once, then in the third step only tri-diagonal systems of small size (e. g., $n_t = 200$) have to be solved. Therefore a typical execution time for this algorithm is in the order of 0.1 seconds.

Observe that due to the fast decay of σ_n, even some time could be saved in the third step by stopping the summation early. This also indicates that increasing the number of grid points n_g will in general not improve the quality of the reconstruction significantly, since components for large n (small σ_n) have only a small impact on the regularized solution.

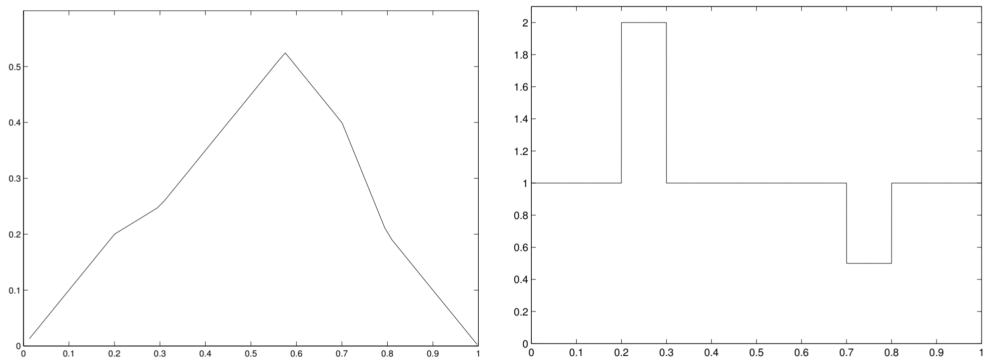

Figure 2: Activation time and corresponding speed of the wave. The speed in healthy tissue is 1, there are two unhealthy regions, with speed 2 and 0.5 respectively.

5 Recovery of the Wave Speed

In the preceding section we have presented an efficient method to recover the electrical potential on the endocardial surface. But as already mentioned in section 3, we cannot expect a precise reconstruction of this potential, due to the exponential decay of the singular values of the forward problem. Furthermore, especially in the 3D-case, the resulting time-dependent solution is difficult to display and to analyze for a physician (e. g., when the physician intends to compare consecutive heart beats). A natural solution to the latter problem is to display the so called *activation time* (see Figure 2), i. e., the time when the cell changes from a resting to an activated state.

Given the potential, there are different methods to derive this activation time $t_a(x)$ at a given point in space, e. g., by recovering the time of maximal potential or maximal slope[2] of the potential [8]. For the case that the shape of the wave with respect to time is only varying slowly, in [23] a cross correlation technique has been presented to determine the activation time.

In the following we present an alternative method, where instead of determining the activation time t_a, we recover the *speed of the wave*, which is given by $1/|\nabla t_a|$ (see Figure 2). Using additional information about the physiological properties of the heart, the speed can be recovered directly, without the necessity of computing the activation time in advance (as opposed to the approach in [23]). The new method can be efficiently implemented also

[2]Note that both values are only vaguely defined for the smooth potentials that are typically recovered.

in 3D and works under the weak assumption that the activation pattern is almost the same for all cells—it is known that this assumption is satisfied well even when the tissue is not healthy (see e. g. [22]). Thus the wave can be described as

$$u(x,t) = h(x, t_a(x) - t) \tag{19}$$

where t_a denotes the activation time of the cell at position x and the activation pattern h varies only slowly in space. Computing the partial derivatives of the potential $u(x,t)$ we obtain

$$\begin{aligned} \frac{\partial u(x,t)}{\partial t} &= h_t(x, t_a(x) - t) \\ \nabla_x u(x,t) &= \nabla_x h(x, t_a(x) - t) + h_t(x, t_a(x) - t) \nabla t_a(x) \end{aligned}$$

Assuming that h_x is negligibly small compared to the second part in the last line we obtain for the speed $v(x)$

$$\begin{aligned} |v(x)| := 1/\left|\nabla t_a(x)\right| &= \frac{\partial u(x,t)}{\partial t} / \left|\nabla_x u(x,t) - \nabla_x h(x, t_a(x) - t)\right| \\ &\approx \frac{\partial u(x,t)}{\partial t} / \left|\nabla_x u(x,t)\right| \end{aligned} \tag{20}$$

i. e., we can recover the speed without knowledge of the function h. Since it is necessary to divide by $|\nabla_x u(x,t)|$, some care has to be taken in this step. The speed does depend on x only, therefore it is possible to multiply (20) with weight functions and integrate with respect to time, in particular we use the equality

$$|v(x)| \int_{t_{\min}}^{t_{\max}} |\nabla u(x,t)| \frac{\partial u(x,t)}{\partial t}\, dt = \int_{t_{\min}}^{t_{\max}} \left(\frac{\partial u(x,t)}{\partial t}\right)^2 dt \tag{21}$$

to compute the speed. In the latter division step a very small penalty is added to avoid divisions by zero (in our examples 1e−10 was used). Observe that in the new approach a differentiation step is involved to obtain the speed, which could in principle introduce additional instabilities. Nevertheless, we only have to differentiate functions which are obtained as solution of (10). Since these are always very smooth and do not contain high-frequency components (see Figure 3) the differentiation does not introduce significant additional error.

To compute the partial derivatives we use a fast method proposed in [25]. The main idea is to use regularized cubic splines to approximate the data and

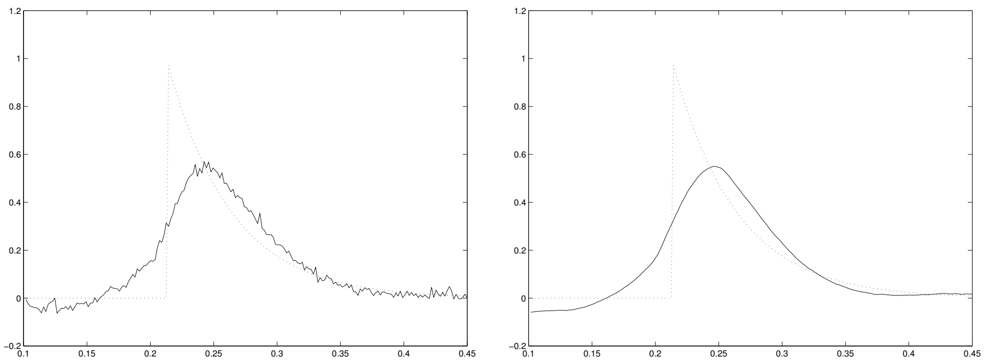

Figure 3: The activation pattern h with respect to time (dashed line) and the reconstructions obtained without (left) and with (right) additional regularization in time.

to use their derivative as approximation to the true derivative. Since only tri-diagonal linear systems have to be solved, the numerical effort for this step is very low. Typical computation times for u_x and u_t are in the order of 0.01 seconds respectively, when the regularization parameter is chosen a-priorily. If the discrepancy principle is used to determine the regularization parameter then the effort increases, since each derivative has to be computed several times. The total effort depends on the initial guess for the regularization parameter and the update strategy, using the globally convergent Newton-type method presented in [13, Chapter 9], this effort can well be kept below 0.2 seconds on our machine (see below).

6 Numerical Examples

In this section we demonstrate the applicability and efficiency of the methods described above on simulated data. All computations were performed on an Intel Pentium M with 1.3GHz and 1.0GB RAM using the software package Matlab. As *activation function* h we choose

$$h(x, t_a(x) - t) = \begin{cases} \exp(-c\,t(x)) & t(x) \geq 0 \\ 0 & t(x) < 0 \end{cases}$$

with $t(x) = t - t_a(x)$ and $c = 20$ (see Figure 3). Note that this function has a jump and is only in $H^{1/2-\varepsilon}$. The *activation time* $t_a(x)$ is shown in Figure 2. It is chosen such that the speed of healthy tissue equals 1, furthermore there are two regions of unhealthy tissue and speed 2 and 1/2 respectively.

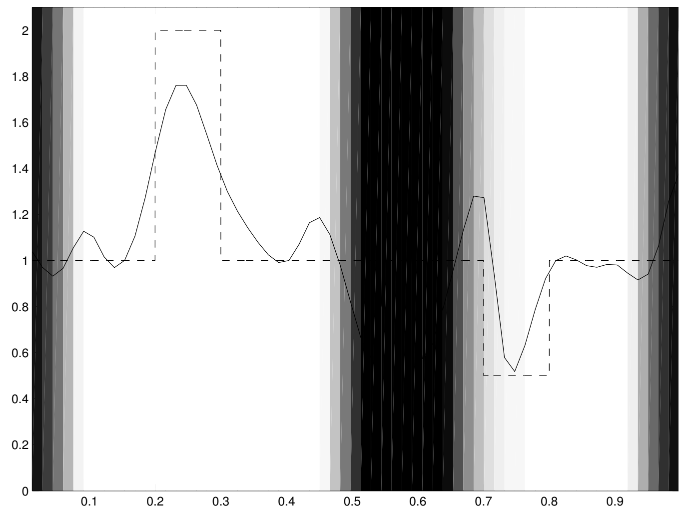

Figure 4: Reconstruction of the speed. The dashed line indicates the exact speed, the black line shows the reconstruction. The lighter the background, the more data were used to compute the result; in black regions no stable reconstruction can be expected, because too few data were available.

To avoid an inverse crime the exact data are generated according to Theorem 2.2, i. e., via a Fourier transform. As discretization level we choose $n_t = 200$ measurements on $n_g = 64$ electrodes. These 200 measurements are then perturbed by 5% Gaussian noise each.

The linear inverse problem is solved via the dynamic method proposed in section 4, where the operator A is generated by a boundary element method (see appendix B). Next, the partial derivatives of the reconstructed potential $u(x, t)$ are computed via the method described in [25] (for the choice of regularization parameters see Remark 6.2).

Figure 4 shows the speed, reconstructed according to (21). To get some qualitative information about the reliability of this reconstruction we use the following simple procedure: For a point x we compute the energy $e(x) := (\int_T u(x,t)^2\,dt)^{1/2}$, which indicates how long the wave was present, and thus how much information is available to recover the speed at this point (cf. Figure 5). The background of Figure 4 is now scaled such that regions with $0 \le e(x) < 1/4 \max(e(x))$ appear black and regions with $3/4 \max(e(x)) \le e(x)$ appear white (see also Remark 6.1).

As Figure 4 shows, in the light regions the speed is recovered in a stable way. In particular, the speed is recovered very well in the interval $[0.7, 0.8]$ where

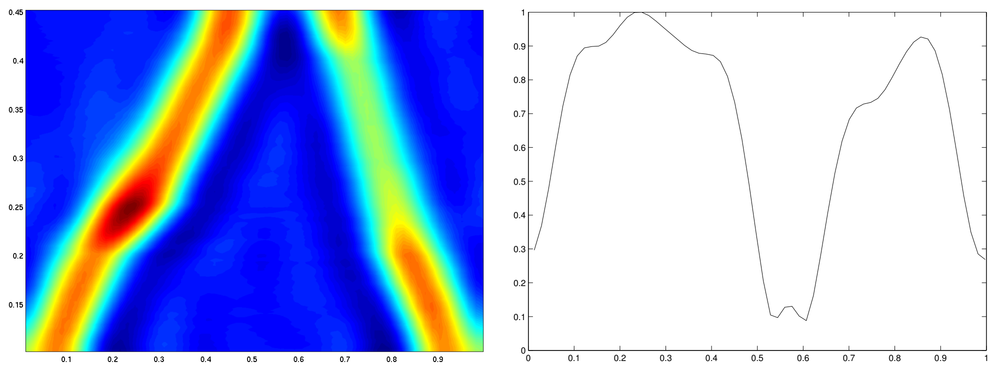

Figure 5: Left: Developement of the potential in time; the regions in the middle and on the borders are hardly hit by the wave. The right plot shows the energy $(\int_T u(x,t)^2\,dt)^{1/2}$.

it is lower than usual. The region with higher speed is also detected, but with less accuracy. A possible explanation for this fact is that due to the higher speed the wave passes faster through this interval, and so there only few data can be collected. Another effect is that the exact potential in the slower region is flatter with respect to time, and can therefore also be better resolved by smooth functions.

The effort for the reconstruction of the speed in Figure 4 is in the order of 0.5 seconds, thus the proposed method yields a good and stable recovery of the essential features in real time.

Remark 6.1 (Data Acquisition). Observe that the exact potential shows a special behavior at two points in time, namely when it emerges from the point $x = 0$ and when it collapses into the point $x = 0.575$ (cf. Figure 5). For these two points no reasonable speed can be defined, moreover, due to regularization the behavior at these points will also interfere with the reconstruction of the speed at points nearby and bias it towards zero. Therefore it is advantageous to discard data that correspond to these points in time, in particular we considered the time-interval $[t_{\min}, t_{\max}]$ with $t_{\min} = 0.1$ and $t_{\max} = 0.45$. In practice this may for instance be done by triggering the data acquisition to an external signal (e. g., an ECG). Caused by this truncation, in Figure 4 regions around the starting and the end point of the wave appear black, at the benefit of a better reconstruction in the white regions.

In the next remark we explain the choice of the regularization parameters.

Remark 6.2 (Regularization Parameters). In formula (12) we set $\beta := \alpha\Delta t$. The value of α is determined via the discrepancy principle with $\tau =$

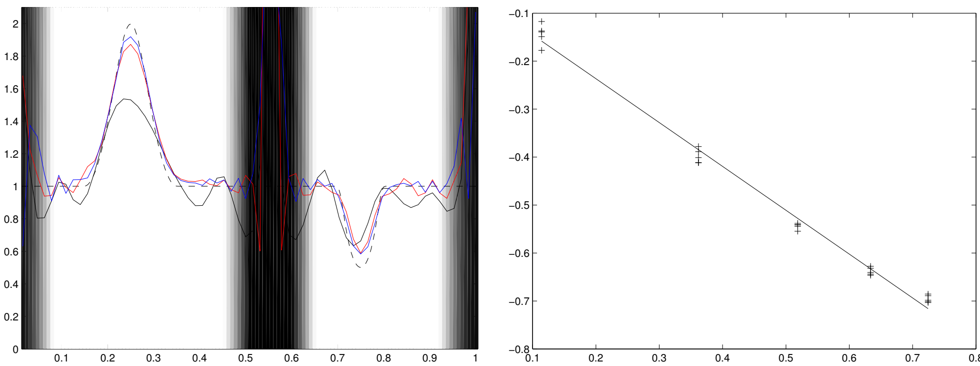

Figure 6: Left: Reconstructions for noise levels 5%, 0.05% and 0.0005%. Right: Dependence of L_2-error in the domain $[0.1, 0.4] \cup [0.65, 0.9]$ on the noise level. The slope of the interpolating line is -0.91.

1.05. In the differentiation step another regularization parameter has to be chosen. We again use the discrepancy principle, now with $\tau = 1.20$. In both cases the residual is measured in the full $L_2(\Gamma_i \times T)$-norm. Observe that only three parameters have to be chosen, in particular, the number of these parameters does not depend on the number of measurements n_t.

This rule for choosing the regularization parameters gives good results for various noise levels as can be seen in Figure 6. As exact speed we choose a function in $H^{5/2-\varepsilon}(\Gamma_o)$. The left plot shows reconstructions with noise levels 5%, 0.05% and 0.0005%. As the noise level decreases, the reconstruction quality improves, although the benefit from decreasing the noise level from 0.05% to 0.0005% is rather small; this is due to the logarithmic convergence rate of the solutions. In the right plot this convergence rate is investigated in detail: for various noise levels the speed is reconstructed and the difference to the exact speed is computed. Since we know that the reconstruction will be bad in the dark regions, we only measure the error in the domain $[0.1, 0.4] \cup [0.65, 0.9]$. The plot shows $\log(\text{error})$ versus $\log(-\log(\delta))$, which exhibits a linear behavior. The slope of the interpolating line is -0.91, i. e., numerically the error behaves as $(-\log(\delta))^{-0.91}$; as for the linear problem (see Theorem 3.2) we obtain a logarithmic convergence rate for the speed, also the exponent is similar. Analogous experiments with the piecewise continuous speed given in Figure 4 yield a numerical convergence rate of $(-\log(\delta))^{-0.40}$.

A Proof of Theorem 3.2

This section is devoted to the derivation of Theorem 3.2. To obtain convergence rates for $\left\|u^\dagger - u_\alpha^\delta\right\|$ when $\delta \to 0$, the least-squares solution $u^\dagger$ has to satisfy a smoothness condition. In the following we discuss smoothness assumptions on $u^\dagger$ and the corresponding attainable convergence rates. The combination of these results will yield Theorem 3.2.

Typically the solution $u^\dagger$ will be piecewise differentiable, but already the first derivative may have jumps. Thus, the proper Sobolev-space for $u^\dagger$ is $H^{3/2-\varepsilon}(\Gamma_o)$. Compared to the smoothing properties of the forward operator (A maps functions in L_2 to analytic functions) this is a rather weak condition on $u^\dagger$. It turns out that therefore for exponentially ill-posed problems *logarithmic source conditions* are appropriate. We define the function

$$\varphi_p(\lambda) := \begin{cases} (-\ln(\lambda/e))^{-p} & 0 < \lambda \leq 1 \\ 0 & \lambda = 0 \end{cases} \tag{22}$$

This function transfers $A^*A : L_2(\Gamma_o) \to C^\infty(\Gamma_o)$ to an operator that maps $L_2(\Gamma_o)$ onto $H^p(\Gamma_o)$, as the following theorem shows.

Proposition A.1. *For $\varphi_p(\cdot)$ as in* (22) *the range of the operator $\varphi_p(A^*A)$ is*

$$\mathcal{R}\left(\varphi_p(A^*A)\right) = H^p(\Gamma_o)\,.$$

Proof. First of all we note that, for $\sigma_n = 2\rho^n(1+\rho^{2n})^{-1}$ and $\varphi_p(\cdot)$ as above, there are constants c, C with

$$0 < c \leq \varphi_p(\sigma_n^2)(1+n^2)^{p/2} \leq C \qquad \text{for} \qquad n = 0, 1, 2, \ldots.$$

For arbitrary $w \in L_2$ we now have

$$\begin{aligned} \|\varphi_p(A^*A)w\|_{H^p}^2 &:= \left\|\sum \varphi_p(\sigma_n^2)\,\langle w,\, v_n\rangle\, v_n\right\|_{H^p}^2 \\ &:= \sum \varphi_p(\sigma_n^2)^2(1+n^2)^p\,|\langle w,\, v_n\rangle|^2 \leq C^2\,\|w\|_{L_2}^2 < \infty. \end{aligned}$$

The second equality is due to the fact that the eigenfunctions of A^*A are just sine and cosine (cf. (3) and (4)) and Parseval's theorem. Altogether we obtain $\mathcal{R}\left(\varphi_p(A^*A)\right) \subseteq H^p$.

To show the converse inclusion we choose some arbitrary $\phi \in H^p$ and define $w := \sum \varphi_p(\sigma_n^2)^{-1} \langle \phi, v_n \rangle v_n$, for which obviously $\varphi_p(A^*A)w = \phi$. This yields

$$
\begin{aligned}
\|w\|_{L_2}^2 &:= \sum \frac{1}{\varphi_p(\sigma_n^2)^2} |\langle \phi, v_n \rangle|^2 \\
&= \sum (1+n^2)^p |\langle \phi, v_n \rangle|^2 \left((1+n^2)^p \varphi_p(\sigma_n^2)^2\right)^{-1} \\
&\leq c^{-2} \|\phi\|_{H^p}^2 < \infty
\end{aligned}
$$

hence $w \in L_2$ and therefore $H^p \subseteq \mathcal{R}\left(\varphi_p(A^*A)\right)$. □

According to this theorem, we obtain that the least-squares solution $u^\dagger$ is in the range of $\varphi_p(A^*A)$, with $p = 3/2 - \varepsilon$. We need this abstract smoothness condition for obtaining convergence rates in the following theorem [21].

Proposition A.2. *Let $u^\dagger \in \mathcal{R}\left(\varphi_p(A^*A)\right)$ for $\varphi_p(\cdot)$ as in* (22) *and α be chosen according to the discrepancy principle* (8)*, then for noise level $\delta \to 0$ we obtain the convergence rate*

$$
\left\|u^\dagger - u_\alpha^\delta\right\| = \mathcal{O}\left(\varphi_p(\delta)\right) .
$$

Theorem 3.2 now follows by combining Proposition A.1 and A.2.

B Boundary Element Method

In the following we describe a boundary integral formulation that can be used in order to numerically implement the operator A in (2).

The potential data taken by the electrodes depend on time, therefore we introduce a time dependence in (IP) and obtain the following boundary value problems for the Laplace equation in the domain Ω (cf. Figure 1):

$$
\begin{aligned}
\Delta u &= 0 && \text{in } \Omega \\
u &= f(x,t) && \text{on } \Gamma_i \times [0,T] \\
\frac{\partial u}{\partial \nu} &= 0 && \text{on } \Gamma_i \times [0,T]
\end{aligned}
\tag{23}
$$

For solving the electrocardial problem it is not necessary to compute $u(x,t)$ in the whole domain $\Omega \times [0,T]$, but already knowledge of $u(x,t)$ on the boundary $\Gamma_o \times [0,T]$ is sufficient. Therefore a boundary integral formulation is the method of choice for recovering $u|_{\Gamma_o \times [0,T]}$, in particular we propose an (indirect) *boundary element method* to solve the problem. In the following we will assume that the boundaries are sufficiently smooth. We look for a solution of (23) via a single layer potential in $\Omega \times [0, T]$, i. e.,

$$\mathcal{S}[(\lambda_o, \lambda_i)](x,t) := \int_{\Gamma_o} \phi(x,y)\lambda_o(y,t)d\gamma(y) + \int_{\Gamma_i} \phi(x,y)\lambda_i(y,t)d\gamma(y),$$

where the *fundamental solution* ϕ is given by

$$\phi(x,y) = \begin{cases} -\frac{1}{2\pi}\log(|x-y|), & \text{2D problems,} \\ \\ \frac{1}{4\pi}\frac{1}{|x-y|}, & \text{3D problems.} \end{cases}$$

and λ_o and λ_i denote *charges* on the inner and outer boundary respectively. These charges will be used in (25) to recover the potential u on Γ_o. Applying the jump properties of the single layer potential [3, 7], we arrive at the following boundary integral equation on $\Gamma_i \times [0, T]$

$$\begin{aligned} &\int_{\Gamma_o}\phi(x,y)\lambda_o(y,t)d\gamma(y) + \int_{\Gamma_i}\phi(x,y)\lambda_i(y,t)d\gamma(y) = f(x,t), \\ &\int_{\Gamma_o}\partial_{n(x)}\phi(x,y)\lambda_o(y,t)d\gamma(y) + \frac{1}{2}\lambda_i(y,t) + \int_{\Gamma_i}\partial_{n(x)}\phi(x,y)\lambda_i(y,t)d\gamma(y) = 0. \end{aligned}$$

In order to obtain a matrix formulation where the potential on the exterior boundary $u_o = u|_{\Gamma_o}$ is the unknown, we introduce the following boundary operators

$$\begin{aligned} \mathcal{V}_{io}[\lambda_o](\,\cdot\,,t) &= \int_{\Gamma_i}\phi(\,\cdot\,,y)\lambda_o(y,t)d\gamma(y) : H^s(\Gamma_o) \to C^\infty(\Gamma_i) \\ \mathcal{V}_{ii}[\lambda_i](\,\cdot\,,t) &= \int_{\Gamma_i}\phi(\,\cdot\,,y)\lambda_i(y,t)d\gamma(y) : H^s(\Gamma_i) \to H^{s+1}(\Gamma_i) \\ \mathcal{K}_{io}[\lambda_o](\,\cdot\,,t) &= \int_{\Gamma_i}\partial_{n(\cdot)}\phi(\,\cdot\,,y)\lambda_o(y,t)d\gamma(y) : H^s(\Gamma_o) \to C^\infty(\Gamma_i) \\ (-\frac{1}{2}\mathcal{I} + \mathcal{K}_{ii})[\lambda_i](\,\cdot\,,t) &= -\frac{1}{2}\lambda_i(\,\cdot\,,t) + \int_{\Gamma_i}\partial_{n(\cdot)}\phi(\,\cdot\,,y)\lambda_i(y,t)d\gamma(y) \end{aligned}$$

where $(-\frac{1}{2}\mathcal{I}+\mathcal{K}_{ii})[\lambda_i](\,\cdot\,,t) : H^s(\Gamma_i) \to H^s(\Gamma_i)$ and all given mapping properties hold for arbitrary $s < \infty$. Operators $\mathcal{V}_{oo}$ and $\mathcal{V}_{oi}$ are defined analogously. Using this setup we obtain the following system of equations

$$\begin{bmatrix} \mathcal{K}_{io} & -\frac{1}{2}\mathcal{I} + \mathcal{K}_{ii} \\ \mathcal{V}_{io} & \mathcal{V}_{ii} \end{bmatrix} \begin{bmatrix} \lambda_o \\ \lambda_i \end{bmatrix} = \begin{bmatrix} 0 \\ f(\cdot,t) \end{bmatrix}, \tag{24}$$

the solution u_o is given in terms of λ_o and λ_i as

$$u_o = \mathcal{V}_{oo}\lambda_o + \mathcal{V}_{oi}\lambda_i\,. \tag{25}$$

Instead of first solving the large system (24) and computing u_o afterwards, we can eliminate the charge variables λ_o and λ_i, leaving u_o as the only unknown, proceeding as follows:

$$\lambda_i = (\frac{1}{2}\mathcal{I} - \mathcal{K}_{ii})^{-1}\mathcal{K}_{io})\lambda_o$$

$$\lambda_o = (\mathcal{V}_{oo} + \mathcal{V}_{oi}(\frac{1}{2}\mathcal{I} - \mathcal{K}_{ii})^{-1}\mathcal{K}_{io})^{-1}u_o \tag{26}$$

$$\lambda_i = (\frac{1}{2}\mathcal{I} - \mathcal{K}_{ii})^{-1}\mathcal{K}_{io})(\mathcal{V}_{oo} + \mathcal{V}_{oi}(\frac{1}{2}\mathcal{I} - \mathcal{K}_{ii})^{-1}\mathcal{K}_{io})^{-1}u_o \tag{27}$$

Finally, defining the linear, one-to-one and smoothing operator $A : H^s(\Gamma_o) \rightarrow C^\infty(\Gamma_i) \subset L_2(\Gamma_i)$, for any $s \in \mathbb{R}$,

$$A := (\mathcal{V}_{io} + \mathcal{V}_{ii}(\frac{1}{2}\mathcal{I} - \mathcal{K}_{ii})^{-1}\mathcal{K}_{io})(\mathcal{V}_{oo} + \mathcal{V}_{oi}(\frac{1}{2}\mathcal{I} - \mathcal{K}_{ii})^{-1}\mathcal{K}_{io})^{-1}, \tag{28}$$

and plugging (26) and (27) in the last row of (24) we arrive at the severely ill-posed problem

$$Au_o(\cdot, t) = f(\cdot, t). \tag{29}$$

In order to reduce (29) to a finite dimensional problem, we can approximate the operator A given in (28) via the approximation of the operators involved in its definition. One possibility is to use spectral approximations of such operators, in order to obtain highly convergent methods; but since we are only given function values on a very coarse grid (64 grid points), *collocation* or *quadrature methods* are more natural for the inverse problem of electrocardiology.

In order to discretize the 2D problem we use the $\frac{1}{6}$-shifted-quadrature method (see [5, 26]) for the operators $\mathcal{V}_{oo}, \mathcal{V}_{ii}$, and Nyström or full-collocation methods [1, 6] for the remaining; substituting the continuous operators in (28) by their approximations, an approximation of the operator A is obtained. Observe that the typical anomaly, which may appear in 2D problems for some special boundaries, can simply be avoided by re-scaling of the domain Ω.

For 3D problems, the theory about boundary element methods based on collocation or quadrature is still not complete, but collocation is the most common method in practical applications with satisfactory results. In [1] and [3] discretizations of the boundary operators $\mathcal{V}_{oo}, \mathcal{V}_{ii}, \ldots$ for 3D problems are given.

Acknowledgements

This work has been supported by the Austrian FWF-Project SFB F 1308, and the Spanish projects MEC / FEDER Ref. MTM 2004-019051 and MCYT / FEDER Ref. BFM 2001-2521.

Furthermore we would like to thank Eric Voth for introducing us into this subject during an "Industrial Problems Study Group" in September 2003 at the Institute for Pure and Applied Mathematics, UCLA. We would also like to thank the staff at IPAM for their hospitality and the organizers of the "Special Semester on Inverse Problems" at IPAM for their invitation.

References

[1] K. Atkinson, *The numerical solution of integral equations of the second kind*, Cambridge University Press, 1997.

[2] A. B. Bakushinskii, *Remarks on choosing a regularization parameter using the quasi-optimality and ratio criterion*, USSR Comp. Math. Math. Phys., 24 (1984), pp. 181–182.

[3] M. Bonnet, *Boundary integral equations methods for solids and fluids*, Wiley, 1999.

[4] D. H. Brooks, G. F. Ahmad, R. S. MacLeod, and G. M. Maratos, *Inverse electrocardiography by simultaneous imposition of multiple constrains*, IEEE Transactions on Biomedical Engineering, 46 (1999), pp. 3–18.

[5] R. Celorrio, V. Domínguez, and F.-J. Sayas, *Periodic Dirac delta distribution in the boundary element method*, Adv. Comput. Math., 17 (2002), pp. 211–236.

[6] R. Celorrio and F.-J. Sayas, *Full collocation methods for some boundary integral equations*, Numerical Algorithms, 22 (1999), pp. 327–351.

[7] G. Chen and J. Zhou, *Boundary element methods*, London Acad. Press, 1992.

[8] L. Chen, J. Bodley, and A. Pullan, *Comparison of potential- and activation-based formulations for the inverse problem of electrocardiol-*

ogy, IEEE Transactions on Biomedical Engineering, 50 (2003), pp. 11–22.

[9] ——, *Effects of experimental and modeling errors on electrocardiographic inverse formulations*, IEEE Transactions on Biomedical Engineering, 50 (2003), pp. 23–28.

[10] P. Colli Franzone, *A mathematical model for cardiac electric sources and related potential fields*, Lecture Notes in Biomathematics. Mathematics in Biology and Medicine, 57 (1983), pp. 220–229.

[11] ——, *Inverse problems in electrocardiology*, Applications of Mathematics in Technology, (1984), pp. 330–339.

[12] H. W. Engl and W. Grever, *Using the L-curve for determining optimal regularization parameters*, Numerische Mathematik, 29 (1993), pp. 25–31.

[13] H. W. Engl, M. Hanke, and A. Neubauer, *Regularization of Inverse Problems*, Kluwer, Dortrecht, 1996.

[14] H. W. Engl and A. Leitao, *A Mann iterative regularization method for elliptic Cauchy problems*, Numer. Funct. Anal. and Optimiz., 22 (2001), pp. 861–884.

[15] W. Freeden, F. Schneider, and M. Schreiner, *Gradiometry - an inverse problem in modern satellite geodesy*, in Inverse Problems in Geophysical Applications, GAMM-SIAM Symposium on Inverse Problems in Geophysics, H. W. Engl, A. K. Louis, and W. Rundell, eds., 1997, pp. 179–239.

[16] F. Greensite, *Remote reconstruction of confined wave front propagation*, Inverse Problems, 11 (1995), pp. 361–370.

[17] ——, *Second-order approximation of the pseudoinverse for operator deconvolutions and families of ill-posed problems*, SIAM Journal on Applied Mathematics, 59 (1998), pp. 1–16.

[18] F. Greensite and G. Huiskamp, *An improved method for estimating epicardial potentials from the body surface*, IEEE Transactions on Biomedical Engineering, 45 (1998), pp. 98–104.

[19] R. M. Gulrajani, *The forward and inverse problems of electro cardiography*, IEEE Engineering in Medicine and Biology, 59 (1998), pp. 84–101.

[20] M. Hanke, *Limitations of the L-curve method in ill-posed problems*, BIT, 36 (1996), pp. 287–301.

[21] T. Hohage, *Regularization of exponentially ill-posed problems*, Numer. Funct. Anal. Optim., 21 (2000), pp. 439–464.

[22] G. Huiskamp and F. Greensite, *A new method for myocardial activation imaging*, IEEE Transactions on Biomedical Engineering, 44 (1997), pp. 433–446.

[23] L. Ji, J. R. McLaughlin, D. Renzi, and J.-R. Yoon, *Interior elastodynamics inverse problems: shear wave speed reconstruction in transient elastography*, Inverse Problems, 19 (2003), pp. S1–S29.

[24] B. Messnarz, B. Tilg, R. Modre, G. Fischer, and F. Hanser, *A new spatiotemporal regularization approach for reconstruction of cardiac transmenbrane potential patterns*, IEEE Trans. Biomed. Eng., 51 (2004), pp. 273–281.

[25] C. H. Reinsch, *Smoothing by spline functions*, Numerische Mathematik, 10 (1967), pp. 177–183.

[26] J. Saranen and L. Schroderus, *Quadrature methods for strongly elliptic equations of negative order on smooth closed curves*, SIAM J. Numer. Anal., 30 (1993), pp. 1769–1795.

[27] U. Schmitt and A. K. Louis, *Efficient algorithms for the regularization of dynamic inverse problems – Part I: Theory*, Inverse Problems, 18 (2002), pp. 645–658.

[28] C. R. Vogel, *Non-convergence of the L-curve regularization parameter selection method*, Inverse Problems, 12 (1996), pp. 535–547.

[29] E. Voth, *A clinical solution of the inverse problem of electrocardiography*, 2003.